Accepted Manuscript

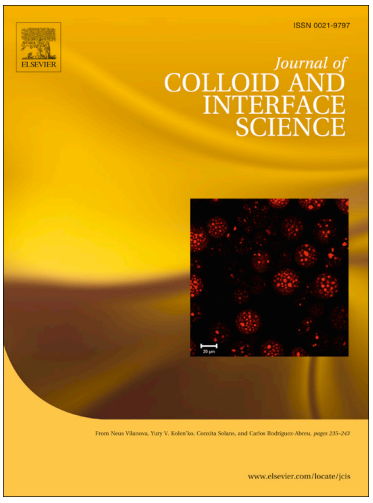

Nanocomposites based on Banana Starch Reinforced with Cellulose Nanofibers Isolated from Banana Peels

Franciele Maria Pelissari, Margarita María Andrade-Mahecha, Paulo José do Amaral Sobral, Florencia Cecilia. Menegalli

PII: S0021-9797(17)30629-X
DOI: http://dx.doi.org/10.1016/j.jcis.2017.05.106
Reference: YJCIS 22413

To appear in: *Journal of Colloid and Interface Science*

Received Date: 7 December 2016
Revised Date: 11 May 2017
Accepted Date: 25 May 2017

Please cite this article as: F.M. Pelissari, M.M. Andrade-Mahecha, P.J. do Amaral Sobral, F.C. Menegalli, Nanocomposites based on Banana Starch Reinforced with Cellulose Nanofibers Isolated from Banana Peels, *Journal of Colloid and Interface Science* (2017), doi: http://dx.doi.org/10.1016/j.jcis.2017.05.106

Nanocomposites based on Banana Starch Reinforced with Cellulose Nanofibers Isolated from Banana Peels

Franciele Maria Pelissari [a,*], Margarita María Andrade-Mahecha [b], Paulo José do Amaral Sobral [c], Florencia Cecilia. Menegalli [d]

[a] Institute of Science and Technology, Food Engineering, University of Jequitinhonha and Mucuri, CEP 39100-000, Diamantina, MG, Brazil.

[b] Departamento de Ingeniería, Universidad Nacional de Colombia, Cra. 32 No. 12-00 Chapinero, Palmira, Valle del Cauca, Colombia.

[c] Department of Food Engineering, School of Food Engineering, University of Campinas, CEP 13083-862, Campinas, SP, Brazil.

[d] Department of Food Engineering, School of Animal Science and Food Engineering, University of São Paulo, CEP 13635-900, Pirassununga, SP, Brazil.

Author information

Corresponding author

***Tel.: +55 38 3532 1200; fax: +55 19 3521 4027.

***E-mail: fpelissari@hotmail.com (F.M. Pelissari).

ABSTRACT

Cellulose nanofibers were isolated from banana peel using a combination of chemical and mechanical treatments with different number of passages through the high-pressure homogenizer (0, 3, 5, and 7 passages). New nanocomposites were then prepared from a mixed suspension of banana starch and cellulose nanofibers using the casting method and the effect of the addition of these nanofibers on the properties of the resulting nanocomposites was investigated. The cellulose nanofibers homogeneously dispersed in the starch matrix increased the glass transition temperature, due to the strong intermolecular interactions occurring between the starch and cellulose. The nanocomposites exhibited significantly increased the tensile strength, Young's modulus, water-resistance, opacity, and crystallinity as the number of passages through the homogenizer augmented. However, a more drastic mechanical treatment (seven passages) caused defects in nanofibers, deteriorating the nanocomposite properties. The most suitable mechanical treatment condition for the preparation of cellulose nanofibers and the corresponding nanocomposite was five passages through the high-pressure homogenizer. In general, the cellulose nanofibers improved the features of the starch-based material and are potentially applicable as reinforcing elements in a variety of polymer composites.

Keywords: banana starch, cellulose nanofibers, high-pressure homogenizer, biodegradable films, mechanical properties.

1. INTRODUCTION

Researchers have sought several alternatives to minimize the environmental impact of conventional polymers, including the use of biodegradable polymers. Because starch is abundant, inexpensive, and degradable, scientists have employed it to produce biodegradable films. However, to technologically apply starch it is necessary to improve its mechanical and barrier properties, because starch films are water-soluble, brittle, and difficult to process. Using nanotechnology to develop films based on polymer nanocomposites containing nanometric fillers might be a new way to improve the mechanical and barrier properties of a given polymer. The reinforcing agent constitutes a nanoparticle when at least one of its dimensions is lower than 100 nm. This particular feature provides unique nanocomposites with outstanding properties that are not seen in conventional composites [1,2].

Among the nanometer-sized fillers, cellulose materials have attracted attention and offer a highly contemporary research line. Cellulose is an abundant polymer in nature and occurs in various plants and living organisms. It is environmentally-friendly, cheap, and biodegradable. Plant-based cellulose nanofibers have generated a great deal of interest because they display large surface to volume ratio, high tensile strength, stiffness, and flexibility, and good dynamic mechanical, electrical, and thermal properties as compared with other commercial fibers [3–5]. The use of cellulose nanofibers as reinforcing elements in matrices improves thermo-mechanical properties, decreases the sensitivity of polymers to water, and preserves biodegradability. Indeed, mixing cellulose nanofibers with polysaccharides (such as starch) improves mechanical properties [6,7].

Because of their annual renewability, agricultural crop residues can be a valuable source of cellulose nanofibers. Researchers have isolated nanostructures from various agricultural residues such as the achira rhizomes [8], pineapple leaf [9], soy hulls [10], wheat straw [11], corn husk [12], coconut husk [13], and sugarcane bagasse [14]. The banana peel waste is a byproduct of the processing of bananas for food products such as banana chips and baby foods. The edible part of the fruit constitutes only 12 wt% of the plant; the remaining parts become agricultural waste and cause environmental problems [15]. Since the banana peel is rich in cellulose, this material is potentially applicable as reinforcing component in high-performance composites, increasing its commercial value and providing a purpose for this byproduct. Agricultural residues from banana crops such as rachis [16,17] and plant wastes [15,18–20] can be used to produce nanoreinforcements.

Several methods based on successive chemical and mechanical treatments can extract highly pure cellulose nanofibers from plant and wood. In high-pressure homogenization, chemically treated dilute slurries of cellulose fibers are pumped at high pressure and fed through a spring-loaded valve assembly. As this valve opens and closes rapidly, the fibers undergo a large pressure drop with shearing and impact forces. This combination of forces promotes high degree of fibrillation of the cellulose fibers, resulting in homogeneous suspensions with more individualized fibers [21,22].

Our previous studies showed that chemical treatment followed by high-pressure homogenization successfully isolates cellulose nanofibers from the banana peel [23,24]. To investigate the potential use of cellulose nanofibers as reinforcing agents in polymers, starch polymer nanocomposites containing these nanofibers were produced and characterized. In order to take full advantage of banana, the pulp was used to obtain the starch that served as matrix for

the films; the peel was employed to isolate the cellulose nanofibers. The resulting nanocomposites were characterized with respect to their mechanical, barrier, optical, structural, and thermal properties.

2. MATERIALS AND METHODS

2.1. Materials

The starch was isolated from unripe plantain bananas (mature green) of the variety "Terra" (*Musa paradisiaca*), according to the methodology described by Pelissari et al. [25] The extracted banana starch reached a purity of 94.8%; 35.0 and 50.3% corresponded to amylose and resistant starch, respectively, in dry basis. All the chemicals employed in this work were reagent grade.

2.2. Isolation of cellulose nanofibers

Cellulose nanofibers were isolated from the banana peel bran using a combination of chemical and mechanical treatments, according to the method described by Pelissari et al. [23]. Firstly, the bran was treated with 5% w/v KOH solution under mechanical stirring at room temperature for 14 h. The insoluble residue was delignified twice with 1% w/v $NaClO_2$ at pH 5.0 at 70 ºC for 1 h, to ensure effective bleaching of the pulp. A second treatment with KOH solution under the same conditions as in the first step was performed. Finally, a 1% v/v H_2SO_4 solution at 80 ºC for 1 h was added to remove mineral traces and to hydrolyze amorphous cellulose.

In order to improve the dispersion of nanofibers, the latter were submitted to mechanical treatment in a two-stage high-pressure homogenizer (GEA Niro Soavi, model NS 1001L – Panda 2K, Parma, Italy). Four nanofiber suspensions were obtained at the end of the procedure; the nanofibers not submitted to homogenization (N0) and those that were passed through the high-pressure homogenizer three (N3), five (N5), and seven (N7) times. Table 1 shows some properties of the obtained nanofibers. The concentration of nanofibers in the suspensions (g of nanofiber/100 g of suspension) was 0.54, 0.48, 0.52, and 0.46 for N0, N3, N5, and N7, respectively. These data were used to prepare the formulation of the nanocomposite films.

2.3. Nanocomposites production

The nanocomposite films were produced by the casting method under process conditions established in preliminary tests [26,27]. The process consisted of drying a film-forming suspension (FFS) that was then applied onto a support. The procedure was according to the methodology described by Andrade-Mahecha [28], and involved the dispersion of nanofiber suspension (5 g of nanofibers/100 g of starch) by magnetic stirring for 20 h, followed by homogenization with an Ultra-Turrax (IKA® Works Inc., model DI 18 Basic, Wilmington, USA) at a speed of 8,000 rpm for 15 min. The nanofiber suspension was added in a water solution of 4 g/100 g (d.b.) of banana starch previously stirred for 15 min. The resulting suspension was homogenized under mechanical stirring for 30 min and heated to the process temperature of 81 ºC. Glycerol (25 g of glycerol/100 g of starch) was added at this point, and the solution was maintained at this temperature for 15 min. Next, the FFS was sonicated for 10 min, and 70 g of the solution was poured onto acrylic plates (18 x 21 cm), to achieve a constant

thickness of 85 ± 5 µm. The nanocomposite films were dried in a chamber with air circulation under controlled temperature (54 ºC) and relative humidity (48%). A control film (without nanofibers) was produced, to evaluate the effect of the addition of cellulose nanofibers.

The nanocomposite films were conditioned in desiccators under 58% RH, at 25 ºC, for 48 h before being characterized for moisture content, mechanical properties, and water vapor permeability. For SEM, XRD, and FTIR analyses, the film samples were cut into small pieces (20 mm x 20 mm) and dehydrated in a desiccator with silica gel (~0% RH) for 3 weeks before being characterized.

2.4. Nanocomposites characterization

2.4.1. Scanning electron microscopy (SEM)

The surface and cross-section of the nanocomposite films were analyzed by SEM for microstructure evaluation. The dried film samples were fractured with the help of tweezers, and small fragments were obtained. Samples of these fragments were fixed on aluminum stubs by means of a double-sided tape and were then coated with a layer of gold (Sputter Coater POLARON, model SC7620), to improve conductivity. The coated samples were viewed under a scanning electron microscope (LEO, model LEO 440i, Cambridge, England) operating at an acceleration voltage of 15 kV.

To identify the chemical elements present in the nanocomposites, analyses were carried out using energy dispersive X-ray spectroscopy (Oxford, model 6070, Cambridge, England) attached to a field emission scanning electron microscope.

2.4.2. Thickness, density, and moisture content

The thickness of the nanocomposites was measured with the aid of a manual micrometer (Fowler, model FOW52-229-001, Pennsylvania, USA) with an accuracy of 0.0001mm. The mean thickness of each film was determined from an average of 10 random measurements.

For determination of the density, samples of each film were cut into 20 x 20 mm squares, and the thickness of these films was measured (3 random measurements). The film samples were dried at 105 ºC for 24 h and weighed, and the density was calculated as the ratio between the weight and volume (thickness x area) of the film. The density experiments were accomplished in triplicate, and the data are reported as mean values.

The moisture content of the films was analyzed gravimetrically, in triplicate, according to the standard method D644-99 [29], by drying the samples at 105 ºC for 24 h.

2.4.3. Mechanical properties

The tensile properties were determined according to the standard method D882-02 [30], by taking an average of six determinations for each sample, and the results are presented as mean values. The samples were cut into 25 mm wide and 115 mm long strips by means of a scalpel and mounted between the tensile grips. The initial grip separation and the crosshead speed were set at 80 mm and 1.0 mm/s, respectively. The tensile strength (force/initial cross-sectional area) and the elongation at break were computed directly from the strength x elongation curves using

the Texture Exponent 32 software, and Young's modulus was calculated as the slope of the initial linear portion of this curve.

2.4.4. Solubility in water

The solubility (*S*) values were calculated by employing the methodology described by Gontard et al. [31]. Initially, three discs (diameter = 20 mm) of each film were stored in a desiccator containing silica gel (~0% RH) for 48 h. The samples were weighed, in order to obtain the initial dry weight (W_i), and they were then immersed into 50 mL water containing sodium azide (0.02% w/v) at 25 ºC for 24 h, under sporadic agitation. After this period, the solution containing the film discs was filtered, the insoluble matter was dried at 105 ºC for 24 h, and the resulting material was weighed for determination of the final dry weight (W_f). Analyses were carried out in quadruplicate, and the solubility in water (%) of the films was computed according to Equation 1:

$$S = \frac{W_i - W_f}{W_i} \times 100 \quad (1)$$

where W_i is the initial dry weight of the sample (g), and W_f is the final dry weight of the sample (g).

2.4.5. Water vapor permeability (WVP)

The WVP was determined gravimetrically by following the standard method E96-00 [32], with modifications, using three different ranges of relative humidity (2 – 33%, 33 – 64%, and 64 – 90%). The film (diameter = 0.06 m) was placed on the circular opening (area = 0.00196 m^2) of a permeation cell and was sealed with sealant ring, to ensure that humidity migration would occur through the film only. The interior of the cell was filled with a salt solution that provided the lower relative humidity (2, 33, or 64%, depending on the case), and the system was stored in a desiccator containing a salt solution that provided higher relative humidity (33, 64, or 90%, depending on the case), at 25 ºC. The weight gain of the cells was monitored every 30 min, for 8 h. Analyses were conducted in triplicate, and the WVP was calculated on the basis of Equation 2 and expressed in g/m.s.Pa:

$$WVP = \frac{w}{t} \times \frac{\delta}{A \cdot \Delta P} \quad (2)$$

where *w/t* is the slope of the line of weight gain (*w*) as a function of time (*t*) graph (g/s), δ is the mean sample thickness (m), *A* is the sample permeation area (m^2), and ΔP is the difference in water vapor pressure through the sample for pure water at 25 ºC (Pa).

2.4.6. Water uptake

The water absorption kinetics was determined according to the methodology described by Dufresne et al. [6]. Nanocomposite films of 20 mm x 20 mm and known thickness, dried at 105 ºC for 24 h, were weighed and conditioned at 25 ºC in hermetically sealed flasks containing Na_2SO_4 saturated solution, to ensure a RH of 95%. The samples were removed at desired

intervals and weighed until the equilibrium state was reached. The water uptake of the samples was calculated using Equation 3:

$$WU = \frac{W_t - W_0}{W_0} \times 100 \quad (3)$$

where *WU* is the water uptake (%), W_t is the weight of the sample after time *t* of exposure to 95% RH (g), and W_0 is the initial weight of the sample (g).

2.4.7. Optical properties

Nanocomposites were subjected to color and opacity analyses using a colorimeter (UltraScan VIS, HunterLab, Virginia, EUA) in the transmittance mode, with the classification system of the CIELab and illuminant D65 (daylight) [33]. The gloss was measured with the aid of a glossmeter (Rhopoint, model Novo-Gloss Lite™, São Paulo, Brazil), following the standard method D523-89 [34]. The gloss values (in gloss units or GU) were obtained in both surfaces of the film; i.e., the side exposed to air during drying (E) and the side in contact with the support plate (I), directly from the equipment in two angles of measurement, namely 20º and 60º. Results are expressed as the arithmetic mean of five measurements on each surface.

2.4.8. X-ray diffraction (XRD)

X-ray diffraction analysis was performed using an X-ray diffractometer (Siemens, model D5005, Baden-Württemberg, Germany) operated at a voltage of 40 kV and a current of 30 mA;

the target was Cu. The diffraction data of the samples were collected over an angular range from 5 to 50º (2θ), at a scanning rate of 1.2º/min. The index crystallinity (%) of the nanocomposites was quantitatively estimated as the ratio of crystalline area to the total area of the diffractogram, by following the method of Nara and Komiya [35] and using the Origin 8.0 software (OriginLab Corporation, Massachusetts, USA).

2.4.9. Fourier-transform infrared spectroscopy (FTIR)

FTIR spectra were recorded on a spectrophotometer (PerkinElmer, model Spectrum One, Ohio, USA) fit with a Universal Attenuated Total Reflectance (UATR) device. Analysis was accomplished in the infrared region, with 16 scans, covering wavenumbers ranging from 4000 to 650 cm^{-1}, with a spectral resolution of 4 cm^{-1} [36].

2.4.10. Differential scanning calorimetry (DSC)

The thermal properties of the films were analyzed on a differential scanning calorimeter (TA-Instruments, model 2920, Pennsylvania, USA) equipped with a cooling system. Prior to the determination, the samples were weighed (7 – 8 mg) in aluminum pans and conditioned in hermetically sealed flasks containing a saturated NaBr solution (58% RH) at 25 ºC, for seven days. For the analysis, the sample pans were hermetically sealed and scanned at a heating rate of 10 ºC/min over a temperature range of -60 to 150 ºC. A sealed, empty aluminum pan was used as reference for all the DSC runs. The glass transition temperature (Tg) was considered to be the inflexion point of the base line, caused by the discontinuity of the specific heat of the sample.

This property was obtained from the thermograms of the samples by using the Universal Analysis 3.9A software. The DSC measurements were performed in triplicate, and the results are presented as mean values.

2.5. Statistical analysis

An analysis of variance (ANOVA) and a Tukey test of multiple comparisons with a significance level of 5% were run using the Statistica 7.0 software (StatSoft Inc, Tulsa, Oklahoma, USA), to compare the differences between the mean values of the properties of the banana starch films reinforced with cellulose nanofibers or not.

3. RESULTS AND DISCUSSION

3.1. Nanocomposites characterization

The nanocomposites based on banana starch and reinforced with cellulose nanofibers isolated from the banana peel presented homogeneous surface with no bubbles or cracks, as well as good handling characteristics. This means that the films could be easily detached from the plates without tearing, and that they were not sticky or too brittle.

3.1.1. Scanning electron microscopy (SEM)

The scanning electron microscopy of the surfaces and cross-sections of the films can be seen in Figure 1. Incorporation of cellulose nanofibers significantly changed the microstructure of the nanocomposites (FN0, FN3, FN5, and FN7) as compared with the control film (FC). Nanocomposites presented non-homogenous structures; i.e., irregular surfaces with imperfections, while the control film displayed a more uniform and smooth surface. Regarding the cross-section, the nanocomposites exhibited less dense and less homogeneous polymeric structures with small cracks, as compared with the control film.

Liu et al. [37] studied the structure of the cellulosic nanocrystals, to find out whether the cellulose microstructure affected the properties of the ordered nanocrystalline phase. The authors rapidly froze a suspension of cellulose nanocrystals in liquid nitrogen and freeze-dried the sample, which furnished foam consisting of cellulose nanocrystals; they also produced a dried film of cellulose nanocrystals using the casting process and characterized both the foam and the film by SEM. The authors verified that the cellulose nanocrystals were self-aligned layer by layer, which afforded an ordered layered structure. When the authors sublimated water from the fibrous network, they obtained foam with ordered, layered, fine micro-sized pore or tube structure; when the authors evaporated water instead of sublimating it, the pore tube structure in the cellulose nanocrystals gel networks collapsed, leading to compact nanofiber layers with ordered fibrous arrangement. Therefore, the cast sample of cellulose nanocrystals became a solid film rather than porous foam. The microstructures of the banana nanocomposites displayed a similar behavior, but the presence of other components such as starch and glycerol in the film formulation culminated in slightly less organized structures consisting of multilayers compacted along the nanocomposite cross-sections.

Each nanofiber had a different aspect ratio, surface charge, and crystallinity (data from Pelissari et al. [23]), as a result of the treatments they underwent during their isolation. These characteristics may account for the type of interactions between cellulose and polymer matrix components (starch, glycerol, and water) and culminate in distinct microstructures. Despite the different structures, the cellulose nanofibers dispersed well in the matrix and did not agglomerate significantly, indicating structural integrity. This is probably a consequence of hydrogen bonding interactions between the hydroxyl groups of the components. The starch matrix coated the nanofibers even after fracture (cross-section), implying that the nanoparticles adhered to the polymer matrix well.

Cellulose nanofibers submitted to mechanical treatment produced nanocomposites (FN3, FN5, and FN7) with rougher surfaces than the nanocomposite containing non-homogenized nanofibers (FN0). The rough areas where nanofibers have been incorporated are more prominent and distinguished in FN3, FN5, and FN7, as well as the smooth areas of starch matrix. Considering that nanoparticles became shorter with increasing number of passages through the high-pressure homogenizer (N0 = 454.9 nm > N3 = 395.6 nm > N5 = 375.2 nm > N7 = 335.1 nm; data from Pelissari et al. [23]), the larger number of cellulose nanofibers per unit area in the films can explain the rougher structures. De Moura et al. [38] also reported similar results for nanocomposites reinforced with cellulose fibers that were successively passed through a microfluidizer.

To determine the chemical elements present in the nanocomposites the spectroscopy analysis by energy dispersive X-ray (EDS) was conducted. The spectra of all the films (Figure 2) confirmed the presence of carbon and oxygen, as expected (the structures of the polymeric matrix and reinforcing material consist of these elements). Small amounts of calcium were

detected in the spectrum of the nanocomposites (FN0, FN3, FN5, and FN7), a result of the chemical treatment employed during isolation of the nanofibers. Thus, calcium salts can be formed during the neutralization steps with chemical reagents, and traces of salts may remain after successive washings of the material.

3.1.2. Thickness, density, and moisture content

The similar thickness values achieved for the films resulted from the strict control of the dry mass content per unit area of plate of the film-forming solutions employed during the casting procedure (Table 2). On the other hand, the incorporation of cellulose nanofibers elicited a statistically significant difference in the density values obtained for the films, with the control film presenting higher density than the nanocomposites ($p < 0.05$; Table 2). The addition of cellulose nanofibers to the nanocomposites affected the density, as a result of the type of microstructure observed in the SEM analysis (Figure 1). The micrographs proved that the structure of the nanocomposites is more open, more porous, and less dense than the structure of the control film. The incorporation of cellulose nanofibers also reduced the moisture content in the nanocomposites (Table 2), because the cellulose nanofibers have lower affinity for water as compared with starch. Müller et al. [39] reported that the moisture content of composites decreased upon addition of cellulose fibers, as observed in this work.

3.1.3. Mechanical properties

Table 3 lists the mechanical properties tensile strength, elongation at break, and Young's modulus of the films; Figure 3 illustrates the corresponding stress-strain curves. Compared with the control film, the tensile strength and Young's modulus of the nanocomposites increased upon addition of cellulose nanofibers, whereas the elongation at break decreased. This means that incorporating cellulose crystallites into the starch matrix results in strong interactions between cellulose crystallites and between cellulose crystallites and the starch matrix, which restrict the chain motion of the starch matrix [40]. The typical curves of tensile properties confirmed that the control film was more flexible; i.e., it had higher elongation at break, and that the nanocomposites were more mechanically resistant. Other authors detected similar behavior for the mechanical characteristics of biodegradable films reinforced with cellulose nanofibers [40–43].

In this study, incorporation of the cellulose nanofibers affected the Young's modulus the most; this parameter increased more than 100% upon addition of the N3 and N5 nanofibers. Helbert et al. [44] attributed this effect to the formation of a fibrillar network within the polymer matrix, the cellulose nanofibers probably interact through hydrogen bonds.

The tensile strength and Young's modulus of the nanocomposites improved with increasing number of passages of nanofibers through the homogenizer, from 0 to 5 passages. This is because the zeta potential of the nanofiber suspensions rose with mechanical treatment (N0 = -16.1 mV < N3 = -28.4 mV < N5 = -36.6 mV < N7 = -44.1 mV; data from Pelissari et al. [23]), preventing the formation of aggregates, giving more stable colloidal suspensions with individualized cellulose fibers, and promoting a strong network of nanofibers inside the material [6,45]. However, after seven passages through the homogenizer, the mechanical resistance of the nanocomposites reinforced with these nanofibers diminished. Given that the lower strength and

stiffness of nanocomposite FN7 is probably due to a brittle fracture, it might be related to the presence of fiber defects that act as crack initiators, and the cracking might be abruptly propagated throughout the nanocomposite. During a more severe mechanical treatment, these defects can be introduced into the nanofibers. Similar results were reported by Nakagaito and Yano [46] for nanocomposites of kraft pulp impregnated with phenolic resin prepared by high-pressure homogenization.

Fibrillated nanofibers play a role in halting cracks in the nanocomposites and contribute to high elongation and strength [4]. In this study, the elongation at break was supposed to be affected by the aspect ratio of the homogenized nanofibers, because nanofibers with low aspect ratio are rigid and easy to pull out from the aggregated fibers. The nanocomposites containing homogenized nanofibers (lower aspect ratio; N3 = 29.4, N5 = 20.8, N7 = 15.1; data from Pelissari et al. [23]) were more brittle than the nanocomposite containing non-homogenized nanofibers (higher aspect ratio; N0 = 42.7; data from Pelissari et al. [23]). Therefore, mechanical treatment shortens the fibers and reduces the elongation at break [47].

3.1.4. Solubility in water

As well known, starch films are hydrophilic due to the chemical composition of starch (amylose and amylopectin), where hydroxyl groups and oxygen bonds with water are formed [48]. Also, the addition of a plasticizer increases the affinity of the material for moisture [49]. Table 4 shows that, except for FN7, all the nanocomposites were less water-soluble (16 – 26% reduction) as compared with the control film. This may be due to (a) better interfacial bonding between the nanofibers, as observed in the SEM studies, (b) greater affinity of the matrix for

water as compared with the nanofibers, and (c) formation of the nanofiber network, which hinders water diffusion through the matrix [50,51].

The incorporation of nanofibers N7 into the starch matrix did not diminish the solubility in water. The defects in nanofibers caused by the drastic mechanical treatment, which would act as crack initiators, probably weakened the nanofiber network inside the material.

3.1.5. Water vapor permeability (WVP)

Table 4 presents the water vapor permeability (WVP) of films in three different gradients of relative humidity (RH): 2 – 33%, 33 – 64%, and 64 – 90%. Unlike conventional plastics, biodegradable films are hygroscopic. Different factors affect film permeability; for instance, the relative humidity to which they are exposed. Studying the WVP of films in different gradients of RH helps assess how well the films promote or inhibit exchange between the product and the environment. In other words, we can identify whether the films are potentially applicable as packaging material [52]. The RH conditions used for film conditioning modify their crystallinity as well as their mechanical and barrier properties [53].

The nanocomposites had lower WVP than the control film in all gradients ($p < 0.05$; Table 4). Reduced WVP elicited by cellulose nanofiber incorporation improved the characteristics of the nanocomposites, considering the hydrophilicity of the matrix. The lower WVP in the presence of cellulose nanofibers agrees with results reported in the case of nanocomposites for packaging applications [42,43,54,55]. Regarding hydrophilic films, WVP is associated with water adsorption and the water diffusion rate [56]. Considering the tortuous pathways theory of composite materials [57,58], the diffusivity rate should decreases in the

presence of the nanofibers, explaining the lower WVP of the nanocomposites. However, the nanoparticles must be fully dispersed in the biopolymer phase and the fibers, and the biopolymer must interact strongly. Thus, the lower WVP of nanocomposites with increasing number of passages through the homogenizer must be due to the fact that the smaller nanofibers were more properly dispersed and entangled inside the matrix than the longer nanofibers. Lower WVP results from the better dispersion and formation of a network of interwoven fibers, because the water molecules have to go through a more tortuous path in the nanocomposites.

The nanocomposite FN5 was less permeable, with WVP reductions of 67, 59, and 77% compared to the control film, for the three RH gradients (Table 4). FN3 and FN5 became less permeable when exposed to the high RH gradient (64 – 90%), as compared with the intermediate RH gradient (33 – 64%). Therefore, these films can be used in products with high moisture content.

Changes in WVP stemming from the effect of the added filler depend on the size and aspect ratio of the filler [58]. The micrographs in Figure 1 reveal that the nanocomposites have a homogeneous matrix, which probably enhanced the ability of the nanofibers to diminish WVP.

3.1.6. Water uptake

The water absorption behavior of nanocomposites was studied at 25 ºC and 95% RH. Figure 4a shows the water uptake for the control film and nanocomposites reinforced with cellulose nanofibers as a function of time. Two well-separated zones are observed: at lower times (zone I: $t < 150$ h), the water absorption kinetics is fast; at times longer than 150 h the water absorption kinetics is slow, resulting in a plateau (zone II). In both zones I and II, the

nanocomposites presented lower water uptake as compared with the control film. Water uptake at equilibrium, M_∞, decreased with increasing number of passages through the homogenizer; the nanocomposite FN5 had the lowest M_∞ (24.91%).

Theoretically, Fick's second law of diffusion (Equation 4) describes water absorption processes in polymer composites; this law has been employed by several authors [6,40,54,59]:

$$\frac{\partial C}{\partial t} = D\left(\frac{\partial^2 C}{\partial x^2}\right) \tag{4}$$

where *C* is the concentration at time *t*, *D* is the diffusion coefficient, and *x* is the coordinate in the thickness direction. The boundary and initial conditions are:

$C = 0, \quad 0 < x < L, \quad t = 0$

$C = C_\infty, \quad x = 0, \quad t > 0$

$C = C_\infty, \quad x = L, \quad t > 0$

Equation 5 gives the general series solution of Fick's second law for plane sheet geometry assuming molecular migration by diffusion, negligible shrinkage, and constant diffusion at short times:

$$\frac{M_t}{M_\infty} = \frac{4}{L}\left(\frac{Dt}{\pi}\right)^{1/2} \tag{5}$$

where M_t and M_∞ are the water contents in the sample at time *t* and at equilibrium, respectively; *L* is the sample thickness; and *D* is the diffusion coefficient that can be calculated from the slope of the linear portion of the curve M_t/M_∞ *vs* $t^{1/2}$ (Figure 4b), where $R^2 \geq 0.99$.

Equation 6 furnishes the sorption coefficient (*S*):

$$S = \frac{m_\infty}{m_p} \quad (6)$$

where m_∞ represents the mass of solvent taken up at the equilibrium and m_p represents the initial dry mass of the sample.

Table 5 summarizes the typical kinetic parameters (M_∞, D, and S). The diffusivity decreases from 2.73×10^{-7} mm^2/s for the control film to 1.71×10^{-7} mm^2/s for the nanocomposite FN5. The high diffusivity of pure starch film stems from its hygroscopic nature, which makes it prone to water absorption. The diffusivity decreases as a function of the addition of nanofibers, reducing water diffusion due to hydrogen bonding between the matrix and the fiber phases within the nanocomposite and increasing tortuosity [60]. Strong hydrogen bonding interactions between starch and cellulose crystallites decrease diffusivity, because these interactions tend to stabilize the starch matrix when the nanocomposites are submitted to high humidity. Reduced water absorption by the film is strongly related to the diminished diffusion coefficient imposed by the nanofibers and to decreased sorption of the penetrant. However, increasing the number of passages of the nanofibers through the homogenizer to above 5 slightly augments diffusivity and the amount of absorbed water (see values for the nanocomposite FN7). Drastic mechanical treatment may have caused defects in nanofibers, reducing matrix cohesion. The interactions between starch and cellulose become weaker, which is detrimental to the barrier properties [61]. Nakagaito and Yano [47] also observed a similar behavior.

3.1.7. Optical properties

All the differences between the control film and the nanocomposites in terms of optical properties were statistically significant ($p < 0.05$; Table 6). Based on the L*, b*, and ΔE* values, the incorporation of cellulose nanofibers produced darker and more yellowish nanocomposites with less uniform color than the control film. The parameter a* values were negative and close to zero for all the films, indicating the absence of characteristic tones of red.

The control film was more transparent than the nanocomposites (Table 6), implying that reinforcement with nanofibers increases opacity (74 to 90%). This phenomenon may result from: (a) nanometer size effects due to the presence of solid particles, (b) strong interactions between the cellulose nanofibers and the starch matrix, (c) high aspect ratio of the cellulose nanofibers, and (d) random distribution of the nanoparticles in the matrix. Increasing number of passages through the homogenizer from 0 to 7 raised the opacity values of the nanocomposites slightly, probably because the homogeneous dispersion of the nanofibers within the composite diminished film transparency. Bilbao-Sainz et al. [54] found that hydroxypropyl methylcellulose films reinforced with cellulose nanofibers behave in the same way; Besbes et al. [45] reported reduced transparency degree for nanofiber suspensions from alpha fibers with increasing number of passages through the high-pressure homogenizer.

Figure 5a depicts the appearance of the nanocomposites reinforced with cellulose nanofibers isolated from the banana peel. Compared with the nanocomposites (Figure 5b), the control film presented higher gloss values, which were more pronounced for the surface exposed to air drying (E). The gloss property is strictly related to surface texture; i.e., to the polishing degree of the analyzed surface [62]. The particle size distribution employed in the film formulation influences this property: more uniform particle size distribution yields more

polished, brighter surfaces [63], justifying the gloss results obtained for the evaluated biodegradable films (remember that cellulose nanofibers have different diameters and length). The higher roughness of the nanocomposites surfaces (Figure 1) also explains the lower gloss values and the higher opacity of these films.

3.1.8. X-ray diffraction (XRD)

The XRD of the nanocomposites was analyzed as a function of the number of passages of the cellulose nanofibers through the high-pressure homogenizer; Figure 6 contains the corresponding diffractograms. The XRD diffractogram of the control film (FC) displayed a typical C-type crystallinity pattern with peaks at 2θ = 5.6º, 12º, 17º, and 20º, typical of B-type, A-type, both A- and B-type, and B-type polymorphs, respectively, corroborating the results obtained for the banana starch film [26]. The crystalline structure results from spontaneous recrystallization or retrogradation of starch molecules after gelatinization. Researchers have frequently detected this phenomenon in starch-based thermoplastic materials [64].

Addition of cellulose nanofibers to the starch matrix furnished a peak at 2θ = 22º, relative to the XRD pattern of cellulose I. Hence, the cellulose nanofibers retained their crystallinity within the matrix [65–67]. The broad peak at 2θ = 12º was absent, which suggests changes in the structure of the nanocomposites.

The presence of cellulose nanofibers altered the XRD patterns of the nanocomposites slightly. The peaks at around 2θ = 5.6º, 17º, and 20º seemed sharper than those of the control film. Increasing the number of passages through the homogenizer from 0 to 7 raised the relative intensity of the peaks, indicating that longer mechanical treatment removed more amorphous

regions in the cellulose nanofibers, corroborating the crystallinity indices (I_c) found for cellulose nanofibers in Pelissari et al. [23] (N0 = 58.6%, N3 = 61.8%, N5 = 62.4%, and N7 = 64.9%). This fact is consistent with the I_c of the films obtained in this study (FC = 13.5%, FN0 = 16.7%, FN3 = 24.4%, FN5 = 26.2 %, and FN7 = 21.8%). Incorporation of cellulose nanofibers increased the I_c of nanocomposites from 24 to 94% compared with the control film, suggesting that the incorporation of highly crystalline fillers enhances the crystallinity of the nanocomposites. Guimarães et al. [68] reported crystallinity values between 20 – 21% for composites based on starch and banana/sugarcane bagasse fibers plasticized with 30 g of glycerol/100 g of starch; Müller et al. [53] obtained crystallinity values of about 50% for cassava starch-cellulose fiber composites (30 g of glycerol/100 g of starch); and Famá et al. [69] found I_c between 11.0 – 13.3% for cassava starch films reinforced with wheat fibers (25 g of glycerol/100 g of starch). Factors such as the relative humidity of composite storage, film formulation, chemical composition, and size and crystallinity of the fibers used as reinforcement affect the crystallinity of these materials.

3.1.9. Fourier transform infrared spectroscopy (FTIR)

FTIR spectra were recorded for the control film and nanocomposites, to compare the types of interactions taking place in the film structures; Figure 7 depicts the spectra. Due to the chemical similarities between starch and cellulose, and to the relatively low content (5 wt%) of nanofibers within the matrix, the nanocomposites exhibited almost the same FTIR spectra as the control film. Increasing number of passages in the high-pressure homogenizer did not influence the spectra of the nanocomposites.

All the films displayed bands at 2927 and 2891 cm^{-1}, corresponding to C–H stretching. The bands at 3300, 1643, and 992 cm^{-1} in the spectra of the films refer to stretching vibrations of the hydrogen bonding –OH groups, bending vibrations of the –OH groups, and stretching vibrations of the C–O in starch, respectively [65].

The band at 1336 cm^{-1} is attributed to bending of the –COH and –CH groups of cellulose in the spectra of the nanocomposites. In the spectrum of the control film, this band is associated with the presence of the amide III group, which was also identified in the spectrum of the banana starch film [26] and related to protein traces that remained in the raw material after extraction. The presence of C–O and C–C groups gives a band at 1150 cm^{-1}. The 1077 cm^{-1} band observed in all the spectra is related to stretching of C–OH bond in the starch [70] and stretching vibrations of C–O in cellulose [17].

The characteristic absorption of cellulose at around 893 cm^{-1} in the spectrum of the nanofibers represents β-glycosidic linkages between the anhydroglucose units in cellulose [71]; this band was absent in the spectra of the nanocomposites. Instead, a band at 851 cm^{-1} was detected and ascribed to the symmetrical stretching of C–O–C bond and CH and CH_2 deformation in the starch. Chen et al. [65] reported similar results for nanocomposites based on pea starch reinforced with cellulose nanofibers from pea hull fiber.

3.1.10. Differential scanning calorimetry (DSC)

Figure 8 shows the DSC curves of the control film and the resulting nanocomposites conditioned at 58% RH. The glass transition temperature (Tg) of the samples is 20.1, 26.8, 29.6, 34.5, and 32.8 ºC for the FC, FN0, FN3, FN5, and FN7, respectively.

The formulation used here consists of a complex heterogeneous system containing glycerol-rich domains dispersed in a starch-rich continuous phase, and each component should exhibit its own Tg. The Tg at 20.1 ºC was associated with the glass transition of the starch-rich phase. However, the Tg of the glycerol-rich phase, located between -80 and -50 ºC, could not be determine because refrigerated cooling of the DSC systems is limited. Incorporation of the cellulose nanofibers into the starch matrix shifted the Tg of the starch-rich phase to higher temperature; from 26.8 to 34.5 ºC. Increased Tg is consistent with the mechanical properties (more rigid and less flexible) and the decreased moisture content of the films upon addition of the nanofiber (Table 2). Water is a plasticizer; diminished water content in the film reduces the plasticizing effect and favors the formation of more thermally stable materials. The mechanical treatment of the cellulose nanofibers also improved the Tg of the nanocomposites; FN5 presented the highest Tg value, probably because the homogenized nanofibers are better distributed in the matrix, promoting more cellulose-starch and cellulose-glycerol interactions.

Several authors have reported increased Tg for films upon addition of cellulose nanofibers [40,64,67]. This is a result of certain factors that occur simultaneously, such as:

(i) Cellulose-water interactions guide the redistribution of water molecules on within the polymer matrix, reducing the plasticizer effect of water [72].

(ii) Strong interactions between the matrix and cellulose nanofibers, mainly between the hydroxyl groups of starch and cellulose, reduce matrix mobility. According to Anglès and Dufresne [73], the amylopectin molecules and reactive cellulose surface have a strong affinity, because both components contain a high density of hydroxyl groups. This coupling effect could culminate in restricted molecular mobility of amylopectin molecules in contact with the

nanofibers surface. Owing to the very high specific surface of cellulose nanofibers, this hindered mobility could be strong enough to affect the global flexibility of the starch matrix.

(iii) Selective partitioning of glycerol within the material in the presence of cellulose nanofibers, with glycerol presenting higher affinity for the cellulose surface than for the starch-based matrix. The main plasticizer migrates from the starch-rich domains toward the filler/matrix interface, decreasing the plasticizing efficiency of glycerol for the starch matrix. This phenomenon should result in increased of Tg and could be more pronounced emphasized in moist conditions [73].

4. CONCLUSIONS

Compared with the control film, the nanocomposites reinforced with cellulose nanofibers present higher tensile strength, Young's modulus, water-resistance, opacity, crystallinity, and thermal stability. The improved performance of the nanocomposites were attributed to (a) the chemical similarities between starch and cellulose, (b) the fact of these components are from the same source, (c) the nanometric size effect of the nanofibers, and (d) the hydrogen bonding interactions between the fillers and the matrix. Regarding the mechanical treatment, as the number of passages through the high-pressure homogenizer increased, the nanocomposites containing homogenized nanofibers (FN3 and FN5) displayed better properties than the nanocomposite produced with the non-homogenized nanofibers (FN0). On the other hand, the drastic mechanical treatment involving seven passages through the homogenizer led to defects in cellulose nanofibers, which act as crack initiators deteriorating the properties of nanocomposite FN7. Hence, we considered that five passages through the homogenizer was the most suitable

condition for the mechanical treatment of cellulose nanofibers, because we obtained nanocomposites with improved features.

Starch and cellulose nanofibers isolated from unripe bananas are potentially applicable as matrix and reinforcing material in biodegradable films, respectively. Furthermore, any agricultural residue, in this case banana peel, can be a source for processing cellulose nanofibers. The nanocomposites produced in this work could find applications in the food packaging industry because they are biocompatible, biodegradable, and non-toxic.

ACKNOWLEDGMENTS

The authors would like to acknowledge the financial support provided by Coordenação de Aperfeiçoamento de Pessoal de Nível Superior (CAPES) (nº 0519/2016-2) and Conselho Nacional de Desenvolvimento Científico e Tecnológico (CNPq) (nº 477842/2011-9 and nº 150523/2013-0).

REFERENCES

[1] H. P. S. A. Khalil, A. H. Bhat, A. F. I. Yusra, Carbohydr. Polym. 87 (2012) 963.

[2] G. Siqueira, J. Bras, A. Dufresne, Biomacromolecules 10 (2009) 425.

[3] L. Brinchi, F. Cotana, E. Fortunati, J. M. Kenny, Carbohydr. Polym. 94 (2013) 154.

[4] M. A. S. A. Samir, F. Alloin, A. Dufresne, Biomacromolecules 6 (2005) 612.

[5] I. Siró, D. Plackett, Cellulose 17 (2010) 459.

[6] A. Dufresne, D. Dupeyre, M. R. Vignon, J. Appl. Polym. Sci. 76 (2000) 2080.

[7] A. Dufresne, M. R. Vignon, Macromolecules 31 (1998) 2693.

[8] M. M. Andrade-Mahecha, F. M. Pelissari, D. R. Tapia-Blácido, F. C. Menegalli, Carbohydr. Polym. 123 (2015) 406.

[9] B. M. Cherian, A. L. Leão, S. F. de Souza, L. M. M. Costa, G. M. de Olyveira, M. Kottaisamy, E. R. Nagarajan, S. Thomas, Carbohydr. Polym. 86 (2011) 1790.

[10] W. P. Flauzino Neto, H. A. Silvério, N. O. Dantas, D. Pasquini, Ind. Crops Prod. 42 (2013) 480.

[11] A. Kaushik, M. Singh, *Carbohydr. Res.* 346 (2011) 76.

[12] C. A. de C. Mendes, N. M. S. Ferreira, C. R. G. Furtado, A. M. F. de Sousa, *Mater. Lett.* 148 (2015) 26.

[13] M. F. Rosa, E. S. Medeiros, J. A. Malmonge, K. S. Gregorski, D. F. Wood, L. H. C. Mattoso, G. Glenn, W. J. Orts, S. H. Imam, *Carbohydr. Polym.* 81 (2010) 83.

[14] E. M. Teixeira, T. J. Bondancia, K. B. R. Teodoro, A. C. Corrêa, J. M. Marconcini, L. H. C. Mattoso, *Ind. Crops Prod.* 33 (2011) 63.

[15] S. Elanthikkal, U. Gopalakrishnapanicker, S. Varghese, J. T. Guthrie, *Carbohydr. Polym.* 80 (2010) 852.

[16] R. Zuluaga, J. L. Putaux, J. Cruz, J. Vélez, I. Mondragon, P. Gañán, *Carbohydr. Polym.* 76 (2009) 51.

[17] R. Zuluaga, J.-L. Putaux, A. Restrepo, I. Mondragon, P. Gañán, *Cellulose* 14 (2007) 585.

[18] B. M. Cherian, L. A. Pothan, T. Nguyen-Chung, G. Mennig, M. Kottaisamy, S. Thomas, *J. Agric. Food Chem.* 56 (2008) 5617.

[19] B. Deepa, E. Abraham, B. M. Cherian, A. Bismarck, J. J. Blaker, L. A. Pothan, A. L. Leao, S. F. de Souza, M. Kottaisamy, *Bioresour. Technol.* 102 (2011) 1988.

[20] X. Mo, Y. Zhong, C. Liang, S. Yu, *Adv. Mat. Res.* 87–88 (2010) 439.

[21] Y. Davoudpour, S. Hossain, H. P. S. A. Khalil, M. K. M. Haafiz, Z. A. M. Ishak, A. Hassan, Z. I. Sarker, *Ind. Crops Prod.* 74 (2015) 381.

[22] F. W. Herrick, R. L. Casebier, J. K. Hamilton, K. R. Sandberg, *J. Appl. Polym. Sci.: Appl. Polym. Symp.* 37 (1983) 797.

[23] F. M. Pelissari, P. J. A. Sobral, F. C. Menegalli, *Cellulose* 21 (2014) 417.

[24] H. Tibolla, F. M. Pelissari, F. C. Menegalli, *LWT – Food Sci. Technol.* 59 (2014) 1311.

[25] F. M. Pelissari, M. M. Andrade-Mahecha, P. J. A. Sobral, F. C. Menegalli, *Starch – Stärke* 64 (2012) 382.

[26] F. M. Pelissari, M. M. Andrade-Mahecha, P. J. A. Sobral, F. C. Menegalli, *Food Hydrocoll.* 30 (2013) 681.

[27] F. M. Pelissari, M. M. Andrade-Mahecha, P. J. A. Sobral, F. C. Menegalli, *LWT – Food Sci. Technol.* 52 (2013) 1.

[28] M. M. Andrade-Mahecha *Microcomposites, nanocomposites and edible coatings based on biodegradable materials from Canna indica L.* PhD thesis, University of Campinas, 2011.

[29] ASTM – D644-99. In: *Annual Book of ASTM Standards.* ASTM: Philadelphia, 1999.

[30] ASTM – D882-02. In: *Annual Book of ASTM Standards.* ASTM: Philadelphia, 2002.

[31] N. Gontard, S. Guilbert, J.-L. Cuq, *J. Food Sci.* 57 (1992) 190.

[32] ASTM – E96-00. In: *Annual Book of ASTM Standards.* ASTM: Philadelphia, 2000.

[33] HunterLab. *Universal software version 3.8. User's manual.* Hunter Associates Laboratory: Reston, 2001.

[34] ASTM – D523-89. In: *Annual Book of ASTM Standards.* ASTM: Philadelphia, 1999.

[35] S. Nara, T. Komiya, *Starch – Stärke* 35 (1983) 407.

[36] N. M. Vicentini, N. Dupuy, M. Leitzelman, M. P. Cereda, P. J. A. Sobral, *Spectrosc. Lett.* 38 (2005) 749.

[37] D. Liu, X. Chen, Y. Yue, M. Chen, Q. Wu, *Carbohydr. Polym.* 84 (2011) 316.

[39] C. M. O. Müller, J. B. Laurindo, F. Yamashita, *Food Hydrocoll.* 23 (2009) 1328.

[40] Y. Lu, L. Weng, X. Cao, *Macromol. Biosci.* 5 (2005) 1101.

[41] H. M. C. Azeredo, L. H. C. Mattoso, D. Wood, T. G. Williams, R. J. Avena-Bustillos, T. H. McHugh, *J. Food Sci.* 74 (2009) N31.

[42] P. R. Chang, R. Jian, P. Zheng, J. Yu, X. Ma, *Carbohydr. Polym.* 79 (2010) 301.

[43] Y. Wang, X. Cao, L. Zhang, *Macromol. Biosci.* 6 (2006) 524.

[44] W. Helbert, J. Y. Cavaillé, A. Dufresne, *Polym. Compos.* 17 (1996) 604.

[45] I. Besbes, M. R. Vilar, S. Boufi, *Carbohydr. Polym.* 86 (2011) 1198.

[46] A. N. Nakagaito, H. Yano, *Appl. Phys. A: Mater. Sci. Process.* 78 (2004) 547.

[47] S. Iwamoto, A. N. Nakagaito, H. Yano, *Appl. Phys. A: Mater. Sci. Process.* 89 (2007) 461.

[48] S. Kuciel, A. Liber-Knec, *J. Biobased Mater. Bioenergy* 3 (2009) 269.

[49] A. P. Mathew, A. Dufresne, *Biomacromolecules* 3 (2002) 609.

[50] V. A. Alvarez, R. A. Ruscekaite, A. Vazquez, *J. Compos. Mater.* 37 (2003) 1575.

[51] M. G. L. Ramírez, K. G. Satyanarayana, S. Iwakiri, G. B. De Muniz, V. Tanobe, T. S. Flores-Sahagun, *Carbohydr. Polym.* 86 (2011) 1712.

[52] G. R. P. Moore, S. M. Martelli, C. Gandolfo, P. J. A. Sobral, J. B. Laurindo, *Food Hydrocoll.* 20 (2006) 975.

[53] C. M. O. Müller, J. B. Laurindo, F. Yamashita, *Carbohydr. Polym.* 77 (2009) 293.

[54] C. Bilbao-Sainz, J. Bras, T. Williams, T. Sénechal, W.Orts, *Carbohydr. Polym.* 86 (2011) 1549.

[55] A. J. Svagan, M. S. Hedenqvist, L. Berglund, *Compos. Sci. Technol.* 69 (2009) 500.

[56] J. J. Kester, O. R. Fennema, *Food Technol.* 40 (1986) 47.

[57] L. E. Nielsen, *Mechanical properties of polymers.* Van Nostrand Reinhold: New York, 1962.

[58] T. J. Pinnavaia, G. W. Beall, *Polymer-clay nanocomposites.* John Wiley & Sons Ltd: New York, 2000.

[59] A. Kaushik, M. Singh, G. Verma, G. *Carbohydr. Polym.* 82 (2010) 337.

[60] M. S. Sreekala, K. Goda, P. V. Devi, *Compos. Interfaces* 15 (2008) 281–299.

[61] M. D. Sanchez-Garcia, E. Gimenez, J. M. Lagaron, *Carbohydr. Polym.* 71 (2008) 235.

[62] I. C. Moraes, G. G. D. Silva, R. A. Carvalho, A. M. Q. B. Habitante, P. V. A. Bergo, P. J. A. Sobral, *Ciênc. Tecnol. Aliment.* 28 (2008) 738.

[63] T. A.Trezza, J. M. Krochta, *J. Appl. Polym. Sci.* 79 (2001) 2221.

[64] X. Cao, Y. Chen, P. R. Chang, M. Stumborg, M. A. Huneault, *J. Appl. Polym. Sci.* 109 (2008) 3804.

[65] Y. Chen, C. Liu, P. R. Chang, X. Cao, D. P. Anderson, *Carbohydr. Polym.* 76 (2009) 607.

[66] T. Nishino, I. Matsuda, K. Hirao, *Macromolecules* 37 (2004) 7683.

[67] Q. Li, J. Zhou, L. Zhang, *J. Polym. Sci. Part B: Polym. Phys.* 47 (2009) 1069.

[68] J. L. Guimarães, F. Wypych, C. K. Saul, L. P. Ramos, K. G. Satyanarayana, *Carbohydr. Polym.* 80 (2010) 130.

[69] L. Famá, L. Gerschenson, S. Goyanes, Starch-vegetable fibre composites to protect food products. *Carbohydr. Polym.* 75 (2009) 230.

[70] J. J. G. Van Soest, H. Tournois, D. de Wit, J. F. G. Vliegenthart, *Carbohydr. Res.* 279 (1995) 201.

[71] A. Alemdar, M. Sain, *Compos. Sci. Technol.* 68 (2008) 557.

[72] A. P. Kumar, R. P. Singh, *Bioresour. Technol.* 99 (2008) 8803.

[73] M. N. Anglès, A. Dufresne, *Macromolecules* 33 (2000) 8344.

Figure captions

Figure 1. SEM surfaces (500x, scale bar = 10 µm; 2000x, scale bar = 3 µm) and cross-sections (2000x, scale bar = 3 µm) of the control film (FC) and nanocomposites reinforced with cellulose nanofibers that were passed through the high-pressure homogenizer zero (FN0), three (FN3), five (FN5), and seven (FN7) times.

Figure 2. EDS spectra of the control film (FC) and nanocomposites reinforced with cellulose nanofibers that were passed through the high-pressure homogenizer zero (FN0), three (FN3), five (FN5), and seven (FN7) times.

Figure 3. Typical stress-strain curves obtained for the control film (FC) and nanocomposites reinforced with cellulose nanofibers that were passed through the high-pressure homogenizer zero (FN0), three (FN3), five (FN5), and seven (FN7) times.

Figure 4. (a) Water uptake during conditioning at 95% RH as a function of time for the control film (FC) and nanocomposites reinforced with cellulose nanofibers that were passed through the high-pressure homogenizer zero (FN0), three (FN3), five (FN5), and seven (FN7) times. (b) Initial part of water absorption curves of the films.

Figure 5. (a) Appearance of the control film (FC) and nanocomposites reinforced with cellulose nanofibers that were passed through the high-pressure homogenizer zero (FN0), three (FN3), five (FN5), and seven (FN7) times. (b) Gloss values of the films, where E is the surface side exposed to air drying and I is the surface side in contact with the support plate. Error bars represent standard deviation of the mean value.

Figure 6. X-ray diffraction patterns of the cellulose nanofibers (NC), control film (FC) and nanocomposites reinforced with cellulose nanofibers that were passed through the high-pressure homogenizer zero (FN0), three (FN3), five (FN5), and seven (FN7) times.

Figure 7. FTIR spectra of the control film (FC) and nanocomposites reinforced with cellulose nanofibers that were passed through the high-pressure homogenizer zero (FN0), three (FN3), five (FN5), and seven (FN7) times.

Figure 8. DSC thermograms of the control film (FC) and nanocomposites reinforced with cellulose nanofibers that were passed through the high-pressure homogenizer zero (FN0), three (FN3), five (FN5), and seven (FN7) times.

Table 1. Characteristics of cellulose nanofibers from banana peel that were passed through the high-pressure homogenizer zero (N0), three (N3), five (N5), and seven (N7) times (data from Pelissari et al. [23]).

Sample	Diameter, D (nm)	Length, L (nm)	Aspect ratio (L/D)	Polydispersity index	Zeta potential (mV)
N0	10.9 ± 2.3^{a}	454.9 ± 6.6^{a}	42.7 ± 7.5^{a}	1.00 ± 0.00^{a}	-16.1 ± 0.7^{a}
N3	14.0 ± 3.7^{ab}	395.6 ± 11.1^{b}	29.4 ± 6.9^{ab}	0.68 ± 0.04^{b}	-28.4 ± 1.7^{b}
N5	18.8 ± 4.6^{ab}	375.2 ± 9.3^{b}	20.8 ± 5.5^{b}	0.56 ± 0.04^{c}	-36.6 ± 1.3^{c}
N7	22.6 ± 4.1^{b}	335.1 ± 6.6^{c}	15.1 ± 2.3^{b}	0.64 ± 0.03^{b}	-44.1 ± 2.1^{d}

^{a,b,c,d} Different letter superscripts in the same column indicate a statistically significant difference ($p < 0.05$).

Table 2. Thickness, density, and moisture content of the control film (FC) and nanocomposites reinforced with cellulose nanofibers that were passed through the high-pressure homogenizer zero (FN0), three (FN3), five (FN5), and seven (FN7) times.

Sample	Thickness (μm)	Density (g/cm^3)	Moisture content (%)
FC	85 ± 1^{a}	1.21 ± 0.01^{a}	15.9 ± 0.4^{a}
FN0	85 ± 1^{a}	1.15 ± 0.01^{b}	15.6 ± 0.2^{ab}
FN3	85 ± 4^{a}	1.17 ± 0.01^{b}	15.2 ± 0.3^{b}
FN5	86 ± 1^{a}	1.17 ± 0.01^{b}	14.9 ± 0.2^{bc}
FN7	86 ± 3^{a}	1.15 ± 0.01^{b}	14.5 ± 0.1^{c}

[a,b,c] Different letter superscripts in the same column indicate a statistically significant difference ($p < 0.05$).

Table 3. Mechanical properties of the control film (FC) and nanocomposites reinforced with cellulose nanofibers that were passed through the high-pressure homogenizer zero (FN0), three (FN3), five (FN5), and seven (FN7) times.

Sample	Tensile strength (MPa)	Elongation at break (%)	Young's modulus (MPa)
FC	7.3 ± 0.5^{a}	32.2 ± 1.4^{a}	478.6 ± 51.3^{a}
FN0	8.9 ± 0.5^{b}	25.9 ± 0.9^{b}	768.6 ± 80.9^{b}
FN3	10.1 ± 0.3^{bc}	21.6 ± 1.3^{c}	966.8 ± 76.0^{c}
FN5	11.1 ± 0.5^{c}	21.4 ± 0.4^{c}	1047.7 ± 13.4^{c}
FN7	9.9 ± 0.4^{bc}	20.7 ± 1.3^{c}	663.1 ± 76.7^{b}

[a,b,c] Different letter superscripts in the same column indicate a statistically significant difference ($p < 0.05$).

Table 4. Solubility in water and water vapor permeability (WVP) of the control film (FC) and nanocomposites reinforced with cellulose nanofibers that were passed through the high-pressure homogenizer zero (FN0), three (FN3), five (FN5), and seven (FN7) times.

Sample	Solubility in water (%)	WVP (10^{-11} g/m.s.Pa)		
		2 – 33%	33 – 64%	64 – 90%
FC	32.3 ± 1.5[a]	10.7 ± 0.1[a]	27.5 ± 0.2[a]	39.5 ± 0.6[a]
FN0	27.2 ± 1.4[bc]	5.7 ± 0.5[b]	16.4 ± 0.4[b]	17.2 ± 0.2[b]
FN3	25.4 ± 1.4[bc]	4.0 ± 0.1[c]	13.0 ± 0.6[c]	12.0 ± 0.6[c]
FN5	23.9 ± 0.9[c]	3.5 ± 0.5[c]	11.2 ± 0.1[d]	8.9 ± 0.7[d]
FN7	29.0 ± 1.6[ab]	6.0 ± 0.1[b]	18.8 ± 0.1[e]	25.4 ± 0.4[e]

[a,b,c,d,e] Different letter superscripts in the same column indicate a statistically significant difference ($p < 0.05$).

Table 5. Barrier properties of the control film (FC) and nanocomposites reinforced with cellulose nanofibers that were passed through the high-pressure homogenizer zero (FN0), three (FN3), five (FN5), and seven (FN7) times.

Sample	M_∞ (%)	D (10^{-7} mm^2/s)	S
FC	30.50 ± 0.27	2.73 ± 0.10	0.42 ± 0.02
FN0	28.48 ± 0.26	2.44 ± 0.05	0.27 ± 0.01
FN3	26.06 ± 0.42	2.05 ± 0.08	0.27 ± 0.01
FN5	24.91 ± 0.33	1.71 ± 0.09	0.16 ± 0.01
FN7	26.15 ± 0.25	2.20 ± 0.12	0.27 ± 0.01

Water content at equilibrium (M_∞), diffusion coefficient (D), and sorption coefficient (S).

Table 6. Optical properties of the control film (FC) and nanocomposites reinforced with cellulose nanofibers that were passed through the high-pressure zero (FN0), three (FN3), five (FN5), and seven (FN7) times.

Sample	L*	a*	b*	ΔE*	Opacity (%)
FC	95.66 ± 0.05^{a}	-0.02 ± 0.01^{a}	0.72 ± 0.01^{a}	0.81 ± 0.04^{a}	26.1 ± 0.5^{a}
FN0	95.14 ± 0.08^{b}	-0.04 ± 0.01^{b}	0.95 ± 0.01^{b}	1.37 ± 0.07^{b}	45.5 ± 0.2^{b}
FN3	95.14 ± 0.04^{b}	-0.04 ± 0.01^{b}	1.01 ± 0.01^{c}	1.39 ± 0.03^{b}	46.2 ± 0.2^{c}
FN5	95.12 ± 0.04^{b}	-0.04 ± 0.01^{b}	1.01 ± 0.01^{c}	1.42 ± 0.04^{b}	49.1 ± 0.4^{d}
FN7	94.99 ± 0.01^{c}	-0.04 ± 0.01^{b}	1.05 ± 0.01^{d}	1.55 ± 0.01^{c}	49.6 ± 0.2^{d}

^{a,b,c,d} Different letter superscripts in the same column indicate a statistically significant difference ($p < 0.05$).

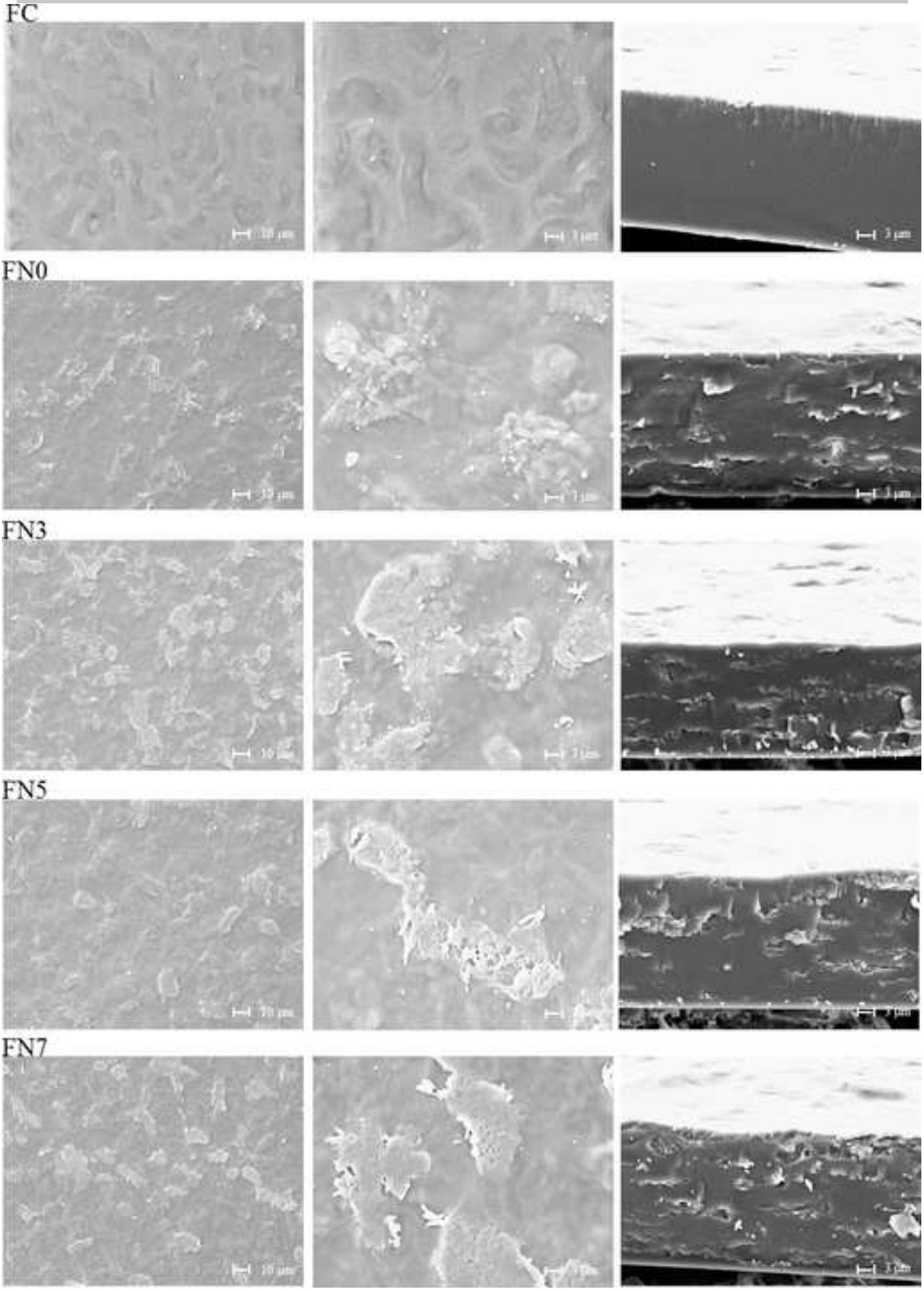

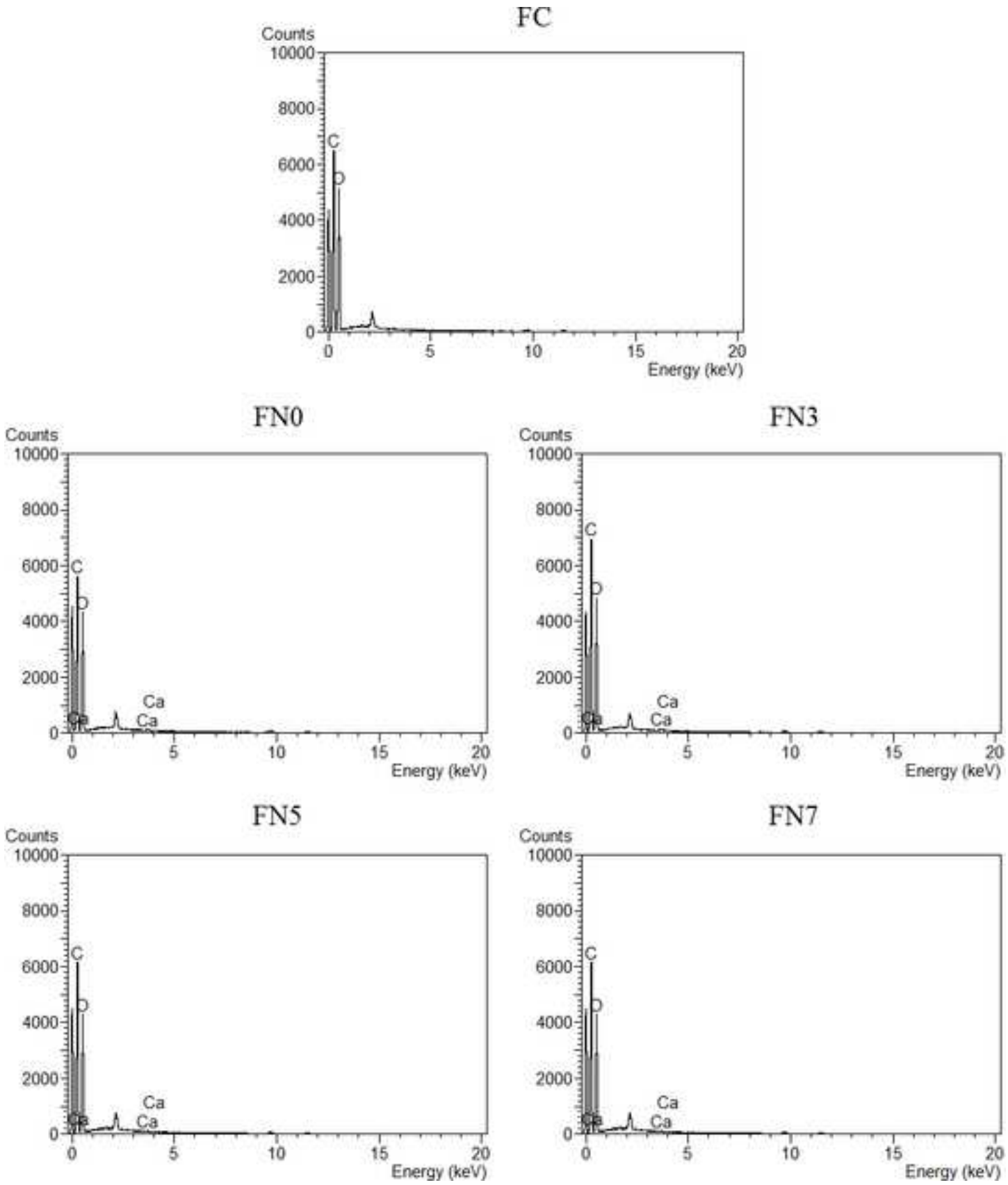

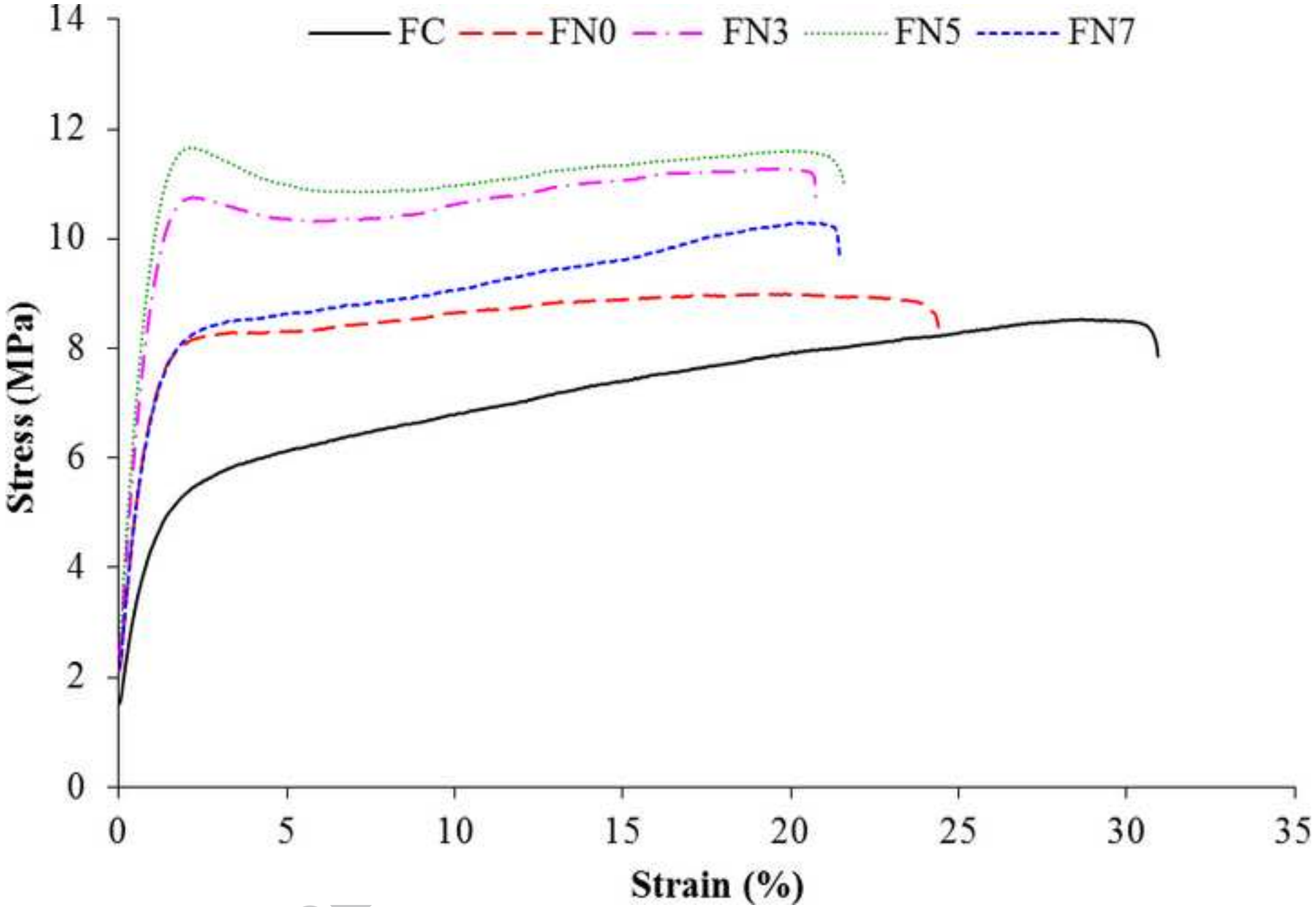

(a)

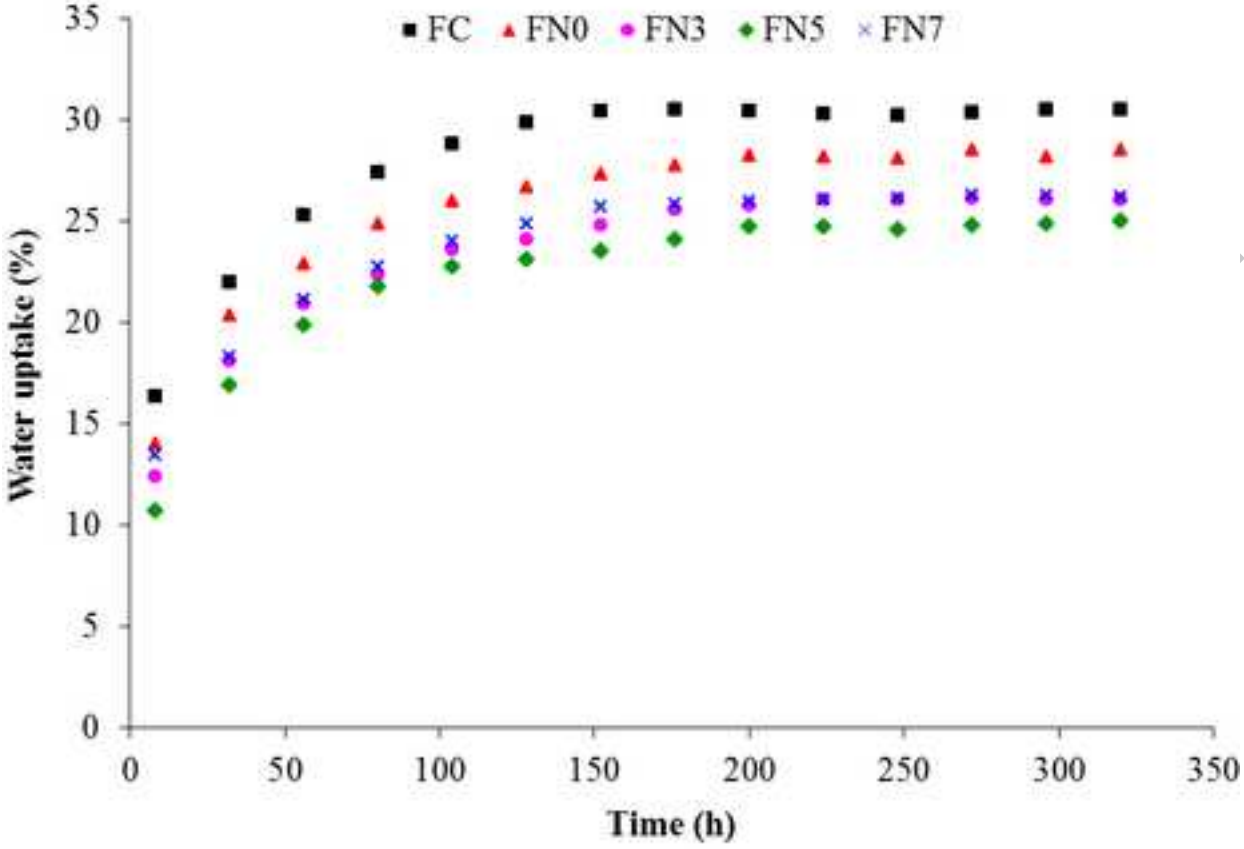

(b)

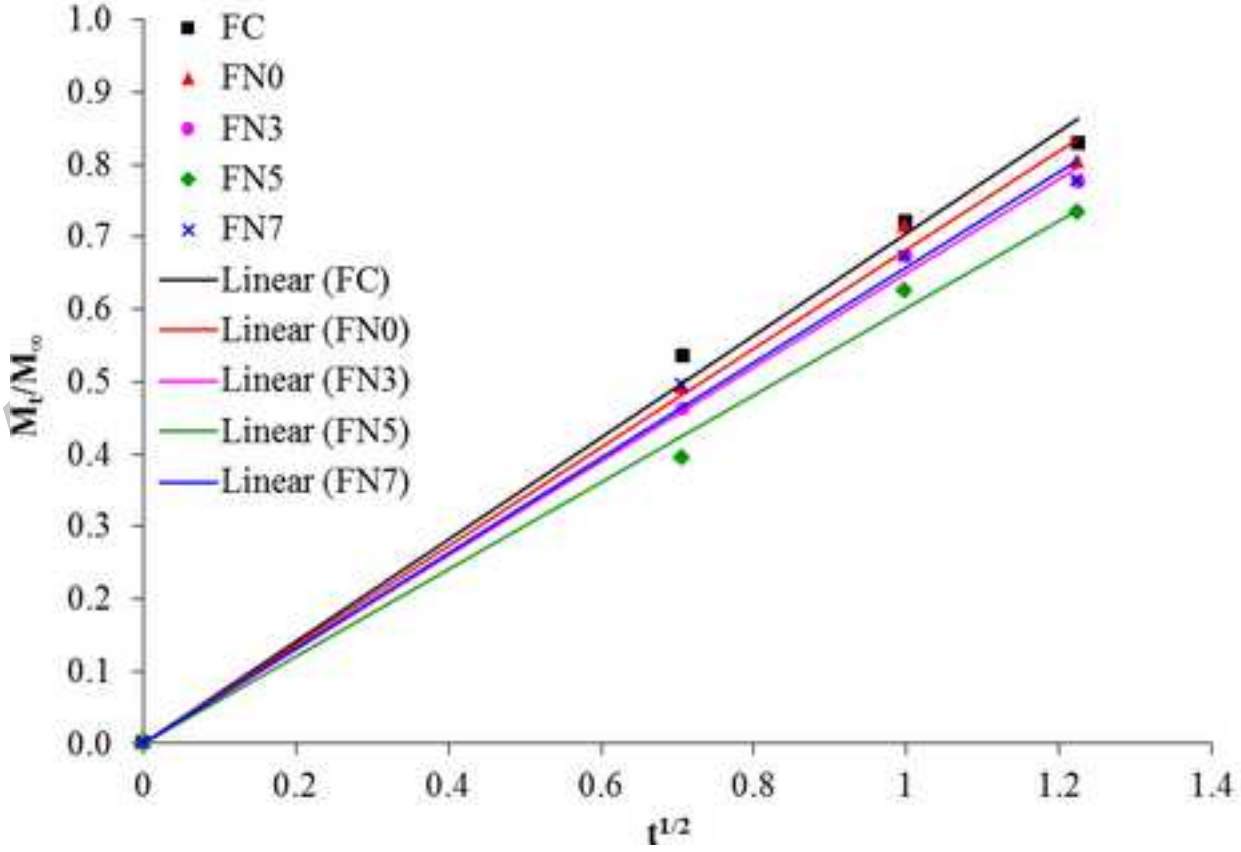

(a)

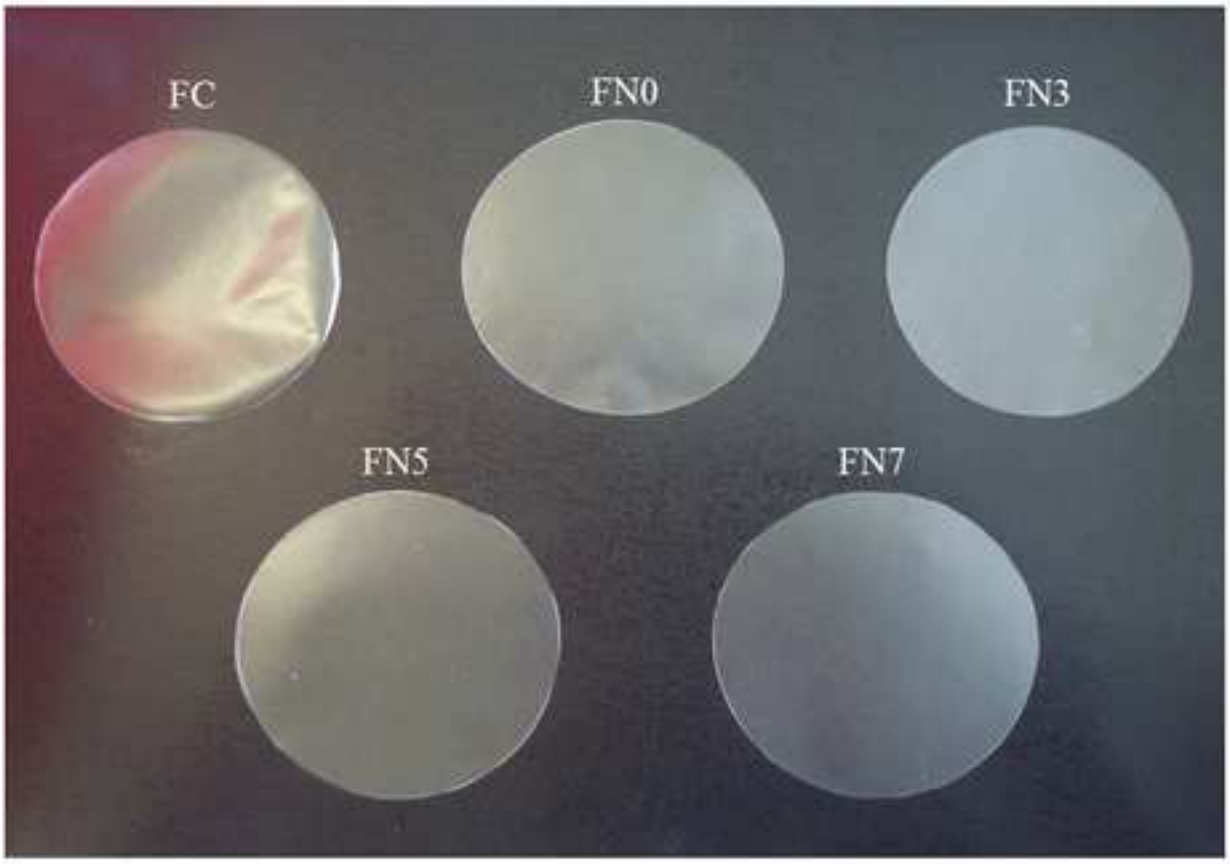

(b)

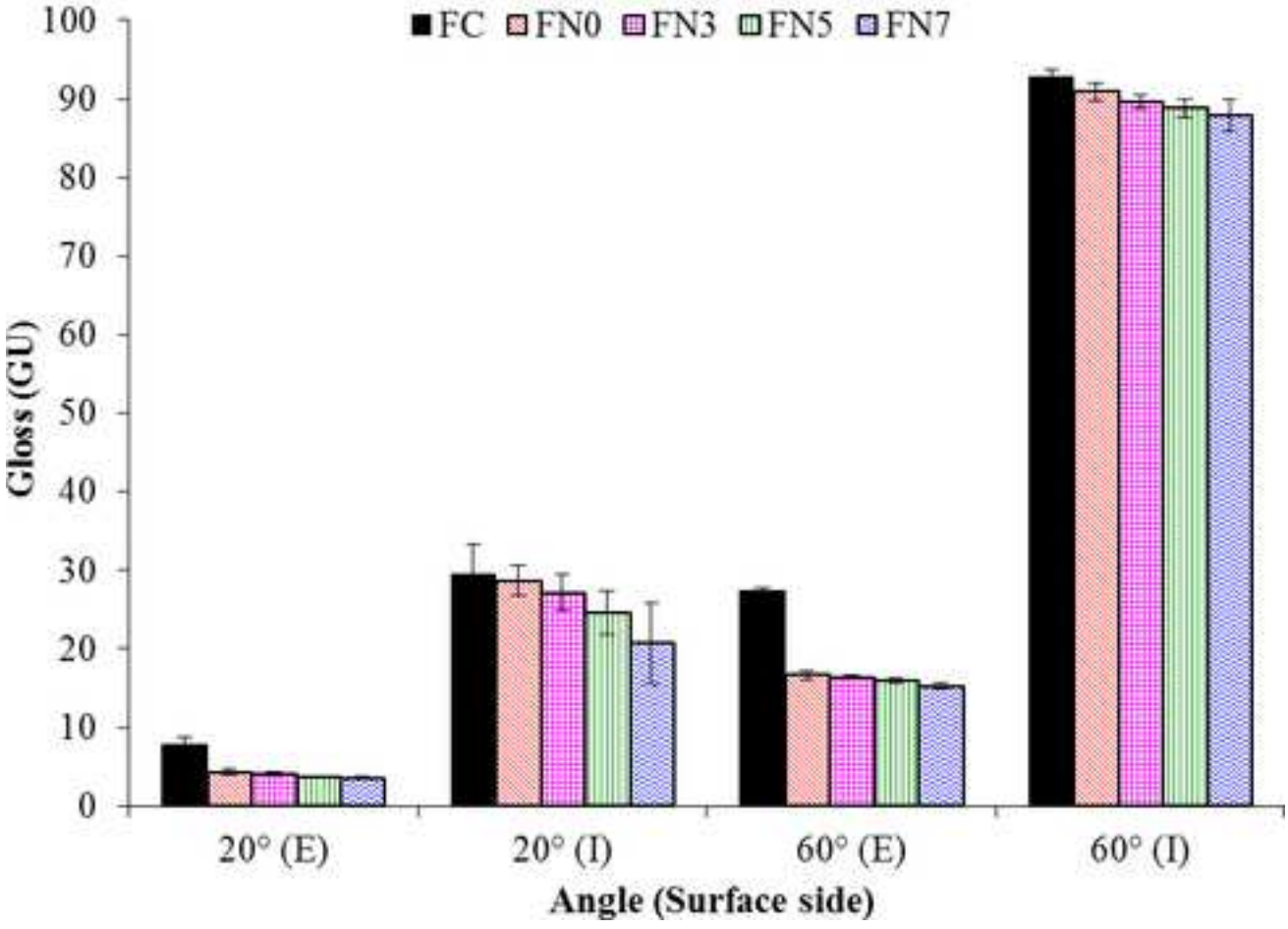

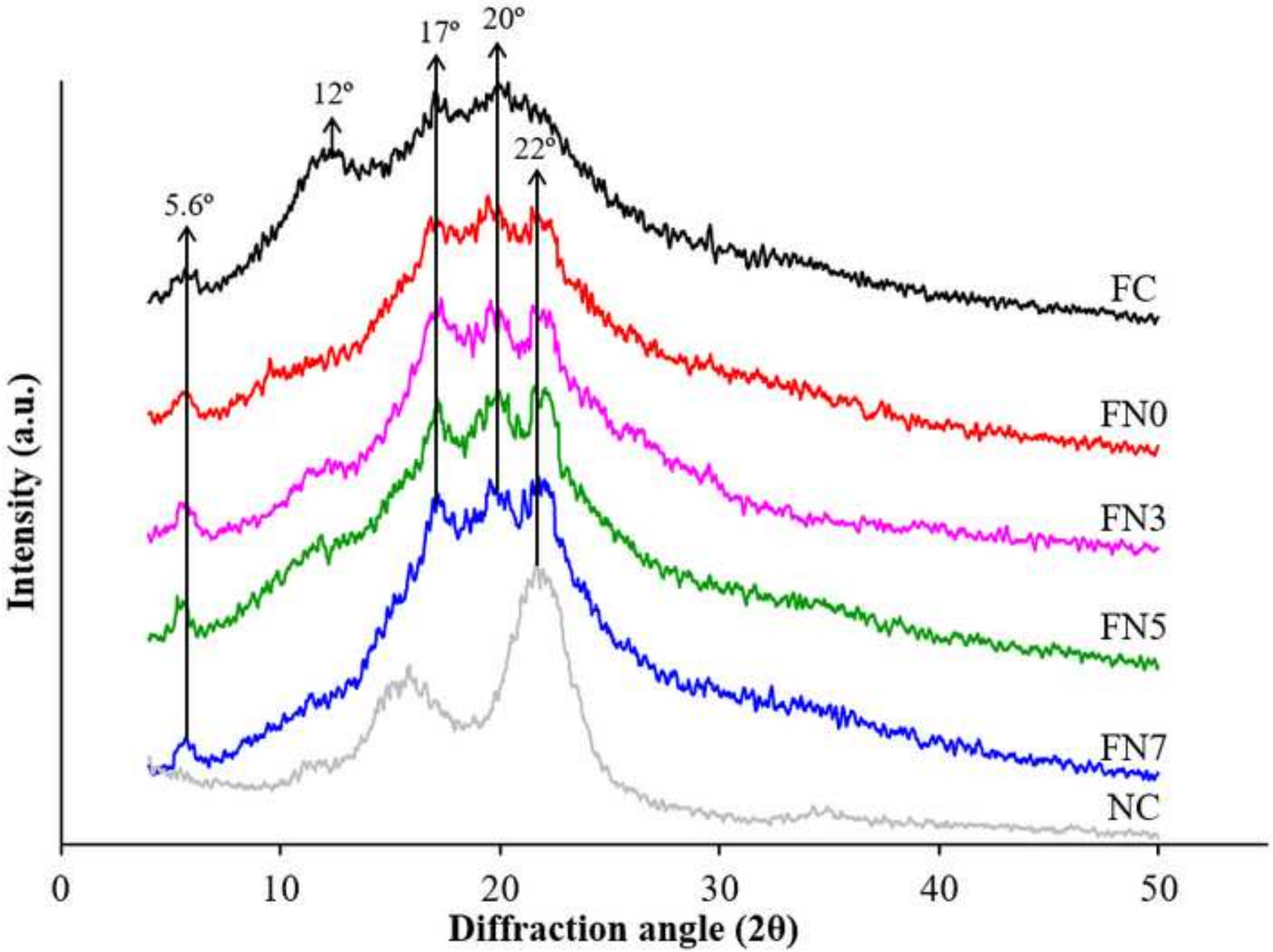

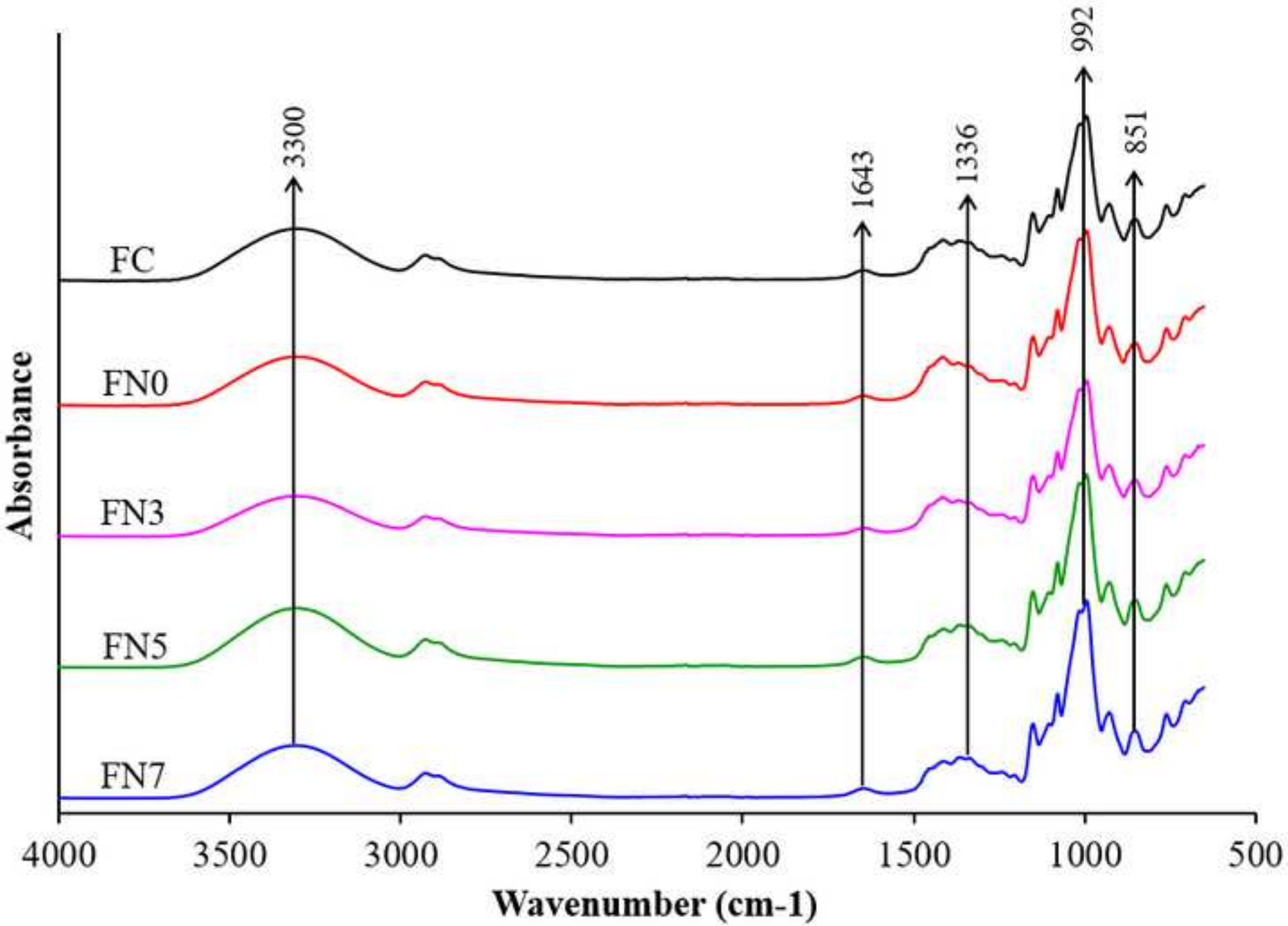

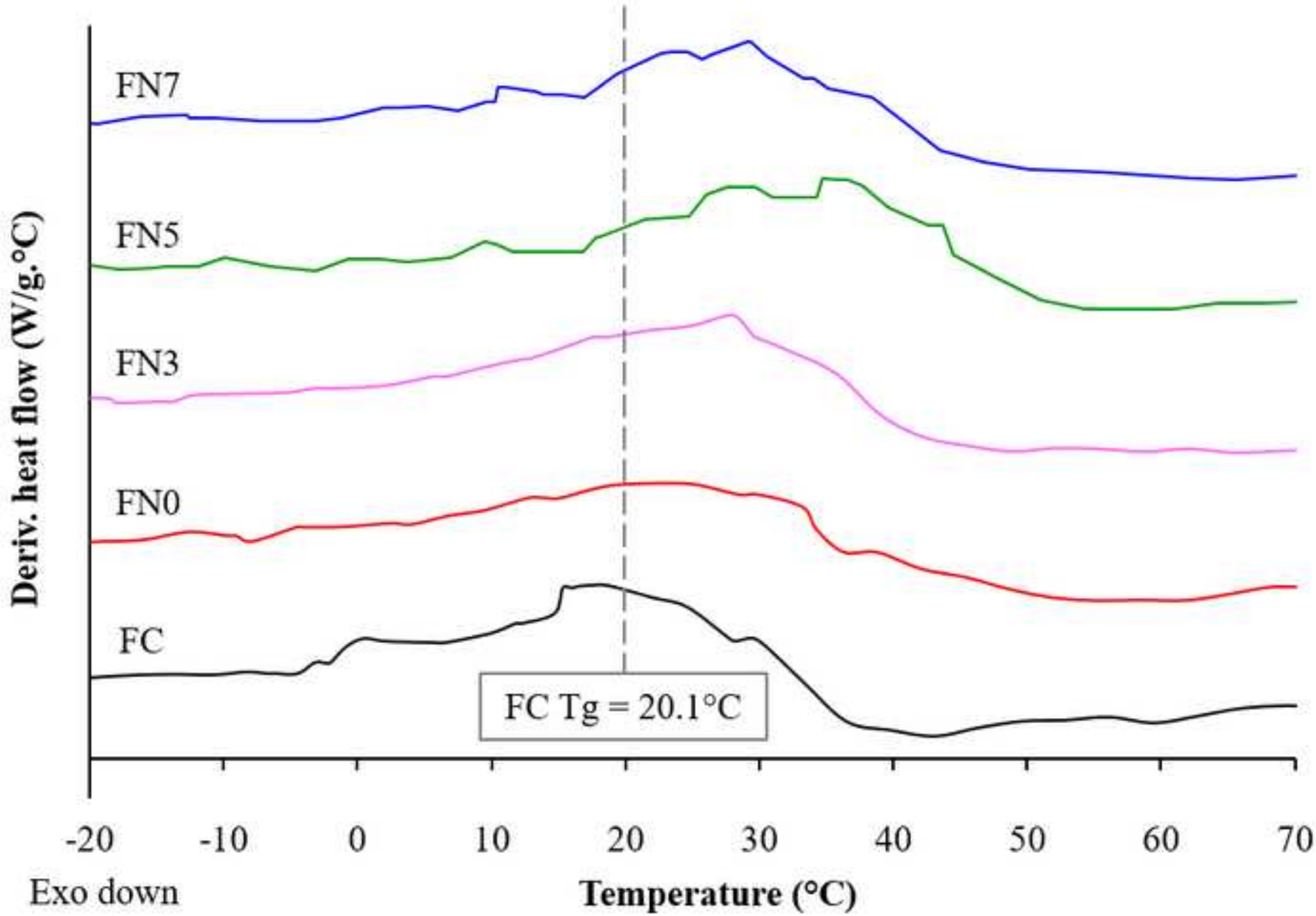

Graphical abstract